

**First Observation of  $\psi(3770) \rightarrow \gamma\chi_{c1} \rightarrow \gamma\gamma J/\psi$** 

T. E. Coan,<sup>1</sup> Y. S. Gao,<sup>1</sup> F. Liu,<sup>1</sup> M. Artuso,<sup>2</sup> C. Boulahouache,<sup>2</sup> S. Blusk,<sup>2</sup>  
 J. Butt,<sup>2</sup> O. Dorjkhaidav,<sup>2</sup> J. Li,<sup>2</sup> N. Menea,<sup>2</sup> R. Mountain,<sup>2</sup> R. Nandakumar,<sup>2</sup>  
 K. Randrianarivony,<sup>2</sup> R. Redjimi,<sup>2</sup> R. Sia,<sup>2</sup> T. Skwarnicki,<sup>2</sup> S. Stone,<sup>2</sup> J. C. Wang,<sup>2</sup>  
 K. Zhang,<sup>2</sup> S. E. Csorna,<sup>3</sup> G. Bonvicini,<sup>4</sup> D. Cinabro,<sup>4</sup> M. Dubrovin,<sup>4</sup> A. Lincoln,<sup>4</sup>  
 R. A. Briere,<sup>5</sup> G. P. Chen,<sup>5</sup> J. Chen,<sup>5</sup> T. Ferguson,<sup>5</sup> G. Tatishvili,<sup>5</sup> H. Vogel,<sup>5</sup>  
 M. E. Watkins,<sup>5</sup> J. L. Rosner,<sup>6</sup> N. E. Adam,<sup>7</sup> J. P. Alexander,<sup>7</sup> K. Berkelman,<sup>7</sup>  
 D. G. Cassel,<sup>7</sup> V. Crede,<sup>7</sup> J. E. Duboscq,<sup>7</sup> K. M. Ecklund,<sup>7</sup> R. Ehrlich,<sup>7</sup> L. Fields,<sup>7</sup> R. S.  
 Galik,<sup>7</sup> L. Gibbons,<sup>7</sup> B. Gittelman,<sup>7</sup> R. Gray,<sup>7</sup> S. W. Gray,<sup>7</sup> D. L. Hartill,<sup>7</sup> B. K. Heltsley,<sup>7</sup>  
 D. Hertz,<sup>7</sup> C. D. Jones,<sup>7</sup> J. Kandaswamy,<sup>7</sup> D. L. Kreinick,<sup>7</sup> V. E. Kuznetsov,<sup>7</sup>  
 H. Mahlke-Krüger,<sup>7</sup> T. O. Meyer,<sup>7</sup> P. U. E. Onyisi,<sup>7</sup> J. R. Patterson,<sup>7</sup> D. Peterson,<sup>7</sup>  
 E. A. Phillips,<sup>7</sup> J. Pivarski,<sup>7</sup> D. Riley,<sup>7</sup> A. Ryd,<sup>7</sup> A. J. Sadoff,<sup>7</sup> H. Schwarthoff,<sup>7</sup> X. Shi,<sup>7</sup>  
 M. R. Shepherd,<sup>7</sup> S. Stroiney,<sup>7</sup> W. M. Sun,<sup>7</sup> D. Urner,<sup>7</sup> T. Wilksen,<sup>7</sup> K. M. Weaver,<sup>7</sup>  
 M. Weinberger,<sup>7</sup> S. B. Athar,<sup>8</sup> P. Avery,<sup>8</sup> L. Brevina-Newell,<sup>8</sup> R. Patel,<sup>8</sup> V. Potlia,<sup>8</sup>  
 H. Stoeck,<sup>8</sup> J. Yelton,<sup>8</sup> P. Rubin,<sup>9</sup> C. Cawfield,<sup>10</sup> B. I. Eisenstein,<sup>10</sup> G. D. Gollin,<sup>10</sup>  
 I. Karliner,<sup>10</sup> D. Kim,<sup>10</sup> N. Lowrey,<sup>10</sup> P. Naik,<sup>10</sup> C. Sedlack,<sup>10</sup> M. Selen,<sup>10</sup> E. J. White,<sup>10</sup>  
 J. Williams,<sup>10</sup> J. Wiss,<sup>10</sup> D. M. Asner,<sup>11</sup> K. W. Edwards,<sup>11</sup> D. Besson,<sup>12</sup> T. K. Pedlar,<sup>13</sup>  
 D. Cronin-Hennessy,<sup>14</sup> K. Y. Gao,<sup>14</sup> D. T. Gong,<sup>14</sup> J. Hietala,<sup>14</sup> Y. Kubota,<sup>14</sup> T. Klein,<sup>14</sup>  
 B. W. Lang,<sup>14</sup> S. Z. Li,<sup>14</sup> R. Poling,<sup>14</sup> A. W. Scott,<sup>14</sup> A. Smith,<sup>14</sup> S. Dobbs,<sup>15</sup>  
 Z. Metreveli,<sup>15</sup> K. K. Seth,<sup>15</sup> A. Tomaradze,<sup>15</sup> P. Zweber,<sup>15</sup> J. Ernst,<sup>16</sup> H. Severini,<sup>17</sup>  
 S. A. Dytman,<sup>18</sup> W. Love,<sup>18</sup> S. Mehrabyan,<sup>18</sup> J. A. Mueller,<sup>18</sup> V. Savinov,<sup>18</sup> Z. Li,<sup>19</sup>  
 A. Lopez,<sup>19</sup> H. Mendez,<sup>19</sup> J. Ramirez,<sup>19</sup> G. S. Huang,<sup>20</sup> D. H. Miller,<sup>20</sup> V. Pavlunin,<sup>20</sup>  
 B. Sanghi,<sup>20</sup> I. P. J. Shipsey,<sup>20</sup> G. S. Adams,<sup>21</sup> M. Anderson,<sup>21</sup> J. P. Cummings,<sup>21</sup>  
 I. Danko,<sup>21</sup> J. Napolitano,<sup>21</sup> Q. He,<sup>22</sup> H. Muramatsu,<sup>22</sup> C. S. Park,<sup>22</sup> and E. H. Thorndike<sup>22</sup>

(CLEO Collaboration)

<sup>1</sup>*Southern Methodist University, Dallas, Texas 75275*<sup>2</sup>*Syracuse University, Syracuse, New York 13244*<sup>3</sup>*Vanderbilt University, Nashville, Tennessee 37235*<sup>4</sup>*Wayne State University, Detroit, Michigan 48202*<sup>5</sup>*Carnegie Mellon University, Pittsburgh, Pennsylvania 15213*<sup>6</sup>*Enrico Fermi Institute, University of Chicago, Chicago, Illinois 60637*<sup>7</sup>*Cornell University, Ithaca, New York 14853*<sup>8</sup>*University of Florida, Gainesville, Florida 32611*<sup>9</sup>*George Mason University, Fairfax, Virginia 22030*<sup>10</sup>*University of Illinois, Urbana-Champaign, Illinois 61801*<sup>11</sup>*Carleton University, Ottawa, Ontario, Canada K1S 5B6**and the Institute of Particle Physics, Canada*<sup>12</sup>*University of Kansas, Lawrence, Kansas 66045*<sup>13</sup>*Luther College, Decorah, Iowa 52101*<sup>14</sup>*University of Minnesota, Minneapolis, Minnesota 55455*<sup>15</sup>*Northwestern University, Evanston, Illinois 60208*<sup>16</sup>*State University of New York at Albany, Albany, New York 12222*<sup>17</sup>*University of Oklahoma, Norman, Oklahoma 73019*<sup>18</sup>*University of Pittsburgh, Pittsburgh, Pennsylvania 15260*

<sup>19</sup>*University of Puerto Rico, Mayaguez, Puerto Rico 00681*

<sup>20</sup>*Purdue University, West Lafayette, Indiana 47907*

<sup>21</sup>*Rensselaer Polytechnic Institute, Troy, New York 12180*

<sup>22</sup>*University of Rochester, Rochester, New York 14627*

(Dated: July 15, 2018)

## Abstract

From  $e^+e^-$  collision data acquired with the CLEO detector at CESR, we observe the non- $D\bar{D}$  decay  $\psi(3770) \rightarrow \gamma\chi_{c1}$  with a statistical significance of 6.6 standard deviations, using the two-photon cascades to  $J/\psi$  and  $J/\psi \rightarrow \ell^+\ell^-$ . We determine  $\sigma(e^+e^- \rightarrow \psi(3770)) \times \mathcal{B}(\psi(3770) \rightarrow \gamma\chi_{c1}) = (18.0 \pm 3.3 \pm 2.5)$  pb and branching fraction  $\mathcal{B}(\psi(3770) \rightarrow \gamma\chi_{c1}) = (2.8 \pm 0.5 \pm 0.4) \times 10^{-3}$ . We set 90% C.L. upper limits for the transition to  $\chi_{c2}$  ( $\chi_{c0}$ ):  $\sigma \times \mathcal{B} < 5.7$  pb ( $< 282$  pb) and  $\mathcal{B} < 0.9 \times 10^{-3}$  ( $< 44 \times 10^{-3}$ ). We also determine  $\Gamma(\psi(3770) \rightarrow \gamma\chi_{c1})/\Gamma(\psi(3770) \rightarrow \pi^+\pi^-J/\psi) = 1.5 \pm 0.3 \pm 0.3$  ( $> 1.0$  at 90% C.L.), which bears upon the interpretation of  $X(3872)$ .

Transitions from  $\psi(3770)$  to other charmonium states are interesting because they test models of  $2^3S_1 - 1^3D_1$  mixing and probe amplitudes for direct transitions from  $1D$  to  $1S$  or  $1P$  states. The latter have been of considerable interest since the discovery of the narrow  $X(3872)$  state in  $\pi^+\pi^-$  transitions to  $J/\psi$  [1, 2] and its possible interpretation as a  $1^3D_2$  state, competing with the  $D\bar{D}^*$  molecule hypothesis. Measurement of hadronic transitions between  $\psi(3770)$  and  $J/\psi$  is a subject of a separate paper [3]. In this Letter, we present an analysis of photon transitions between  $\psi(3770)$  and  $\chi_{cJ}(1P)$  states, followed by another photon transition to  $J/\psi$ , with  $J/\psi$  decaying to  $e^+e^-$  or  $\mu^+\mu^-$ .

The data were acquired at a center-of-mass energy of 3773 MeV with the CLEO-c detector [4] operating at the Cornell Electron Storage Ring (CESR), and correspond to an integrated luminosity of  $281 \text{ pb}^{-1}$ . The CLEO-c detector features a solid angle coverage of 93% for charged and neutral particles. The cesium iodide (CsI) calorimeter attains photon energy resolutions of 2.2% at  $E_\gamma = 1 \text{ GeV}$  and 5% at 100 MeV. For the data presented here, the charged particle tracking system operates in a 1.0 T magnetic field along the beam axis and achieves a momentum resolution of 0.6% at  $p = 1 \text{ GeV}/c$ .

We select events with exactly two photons and two oppositely charged leptons. The leptons must have momenta of at least 1.4 GeV. We distinguish between electrons and muons by their energy deposition in the calorimeter. Electrons must have a high ratio of energy observed in the calorimeter to the momentum measured in the tracking system ( $E/p > 0.7$ ). Muons are identified as minimum ionizing particles, thus required to leave 150 – 550 MeV of energy in the calorimeter. Stricter lepton identification does not reduce background in the final sample, since all significant background sources contain leptons. Each photon must have at least 60 MeV of energy and must be detected in the barrel part of the calorimeter, where the energy resolution is best. The invariant mass of the two photons must be at least 3 standard deviations away from the nominal  $\pi^0$  or  $\eta$  mass. The total momentum of all photons and leptons in each event must be balanced to within 50 MeV. The invariant mass of the two leptons must be consistent with the  $J/\psi$  mass within  $\pm 40$  MeV. The measured recoil mass against two photons is required to be within  $-4$  and  $+3$  standard deviations from the  $J/\psi$  mass. An average resolution of the recoil mass is 16 MeV. To reduce Bhabha background in the dielectron sample we require an average of the cosines of the angle between the electron direction and the direction of the electron beam and of the angle between the positron direction and the direction of the positron beam to be less than 0.5. The event selection efficiencies for  $\psi(3770) \rightarrow \gamma\chi_{cJ}$ ,  $\chi_{cJ} \rightarrow \gamma J/\psi$ ,  $J/\psi \rightarrow \mu^+\mu^-$  ( $J/\psi \rightarrow e^+e^-$ ) events are 23%, 29% and 25% (13%, 17% and 15%) for the  $\chi_{c2}$ ,  $\chi_{c1}$  and  $\chi_{c0}$  states, respectively.

After all selection cuts, we employ kinematic fitting of events to improve resolution on the photon energy. We constrain the total energy and cartesian components of total momentum to the expected center-of-mass four-vector components, which take into account a small beam crossing angle. We also impose a  $J/\psi$  mass constraint. No cut on confidence level of the kinematic fit is used, since the explicit selection cuts on the constrained quantities have been already employed, as described above, and because the calorimeter energy response function is not Gaussian. These constraints improve energy resolution for the first transition photon by 20%. The effect of kinematic fitting is illustrated on the CLEO-c  $\psi(2S)$  data ( $1.5 \times 10^6$  resonant decays) in Fig. 1. These data have clean  $\psi(2S) \rightarrow \gamma\chi_{c2,1}$  signals in  $\gamma\gamma\ell^+\ell^-$  events, which we selected with the same criteria as described above. The separation between these two photon lines improves after the kinematic constraints and the detector response function becomes Gaussian. To verify our selections and procedures, branching fractions for  $\psi(2S) \rightarrow \gamma\chi_{cJ} \rightarrow \gamma\gamma J/\psi$  decays are determined from a fit to the kinematically-constrained

photon energy distribution (Fig. 1b). The normalizations, widths and positions of two Gaussian shapes representing large  $\chi_{c2,1}$  signals, the normalization of small  $\chi_{c0}$  signal (with its shape fixed to the shape of the Monte Carlo distribution), and polynomial-background parameters float in this fit. This cross-check gives results that are within (1–2)% (relative) of the recently published [5] analysis using different selections and signal extraction techniques.

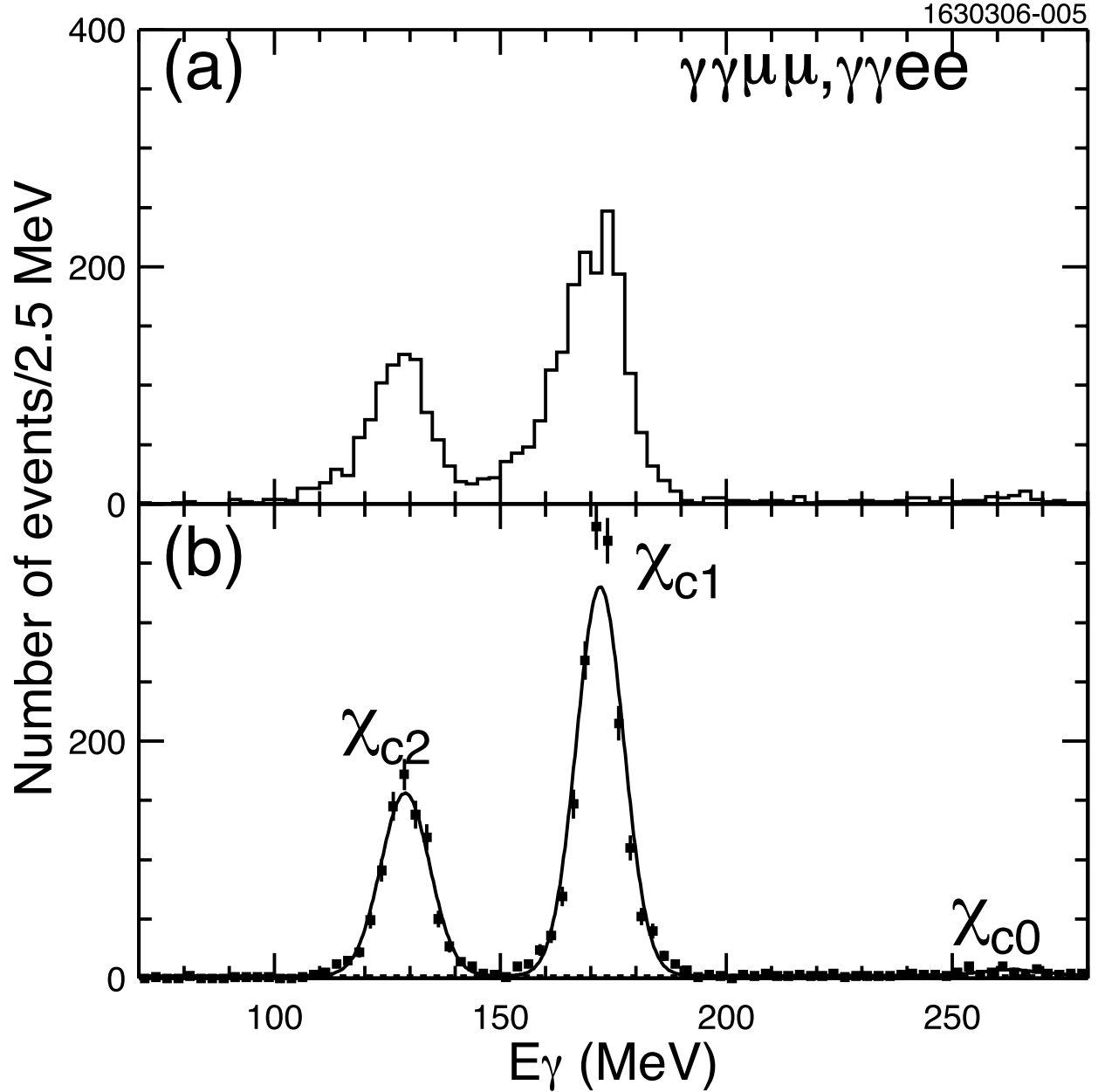


FIG. 1: Energy of the lower energy photon for  $\psi(2S) \rightarrow \gamma\chi_{cJ} \rightarrow \gamma\gamma J/\psi$ ,  $J/\psi \rightarrow \ell^+\ell^-$  events in the CLEO-c data; (a) before and (b) after kinematic constraints on the events (see text). The solid line in the bottom plot represents the fit of the  $\chi_{cJ}$  signals on top of barely visible polynomial background (dashed line).

The photon energy distribution for the lower energy photon in the event is plotted for  $\psi(3770) \rightarrow \gamma\chi_{cJ} \rightarrow \gamma\gamma J/\psi$ ,  $J/\psi \rightarrow \ell^+\ell^-$  Monte Carlo data in Fig. 2. Transitions via the

$\chi_{c2}$  and  $\chi_{c1}$  states produce Gaussian distributions peaked at the photon energies generated in  $\psi(3770) \rightarrow \gamma\chi_{c2,1}$  decays. Transitions via the  $\chi_{c0}$  state produce a broad distribution since the lower energy photon is usually due to the Doppler broadened  $\chi_{c0} \rightarrow \gamma J/\psi$  photon line, and sometimes due to  $\psi(3770) \rightarrow \gamma\chi_{c0}$  decay, as these two photon lines overlap each other.

We fit the distribution observed in the data with these three signal contributions on top of a smooth background represented by a quadratic polynomial. The  $\chi_{c2,1}$  signals are represented by Gaussian peaks. The widths of the signal peaks are fixed to the values predicted by the Monte Carlo simulations ( $\sigma_{E_\gamma} = 5.1$  MeV). Amplitudes of both Gaussians and the energy of the  $\chi_{c1}$  peak are free parameters in the fit. The energy of the  $\chi_{c2}$  peak is constrained to be the latter minus the mass difference between these two states. The  $\chi_{c0}$  signal shape is fixed to the Monte Carlo distribution (Fig. 2).

In addition to  $e^+e^- \rightarrow \psi(3770)$ ,  $\psi(3770) \rightarrow \gamma\chi_{cJ}$ , also  $e^+e^- \rightarrow \gamma\psi(2S)$ ,  $\psi(2S) \rightarrow \gamma\chi_{cJ}$  can contribute to the observed peaks. The cross section for the latter process peaks for small energies of the initial state radiation photon. Hence the produced  $\psi(2S)$  mass from the high-mass tail of this resonance peaks at the center-of-mass energy. This makes the  $\psi(2S)$  background indistinguishable from the  $\psi(3770)$  signal. We estimate the size of this background from the theoretical formulae, which fold in radiative flux,  $W(s, x)$ , the Breit-Wigner shape of  $\psi(2S)$ ,  $BW(s')$ , the branching ratio,  $\mathcal{B}_X$ , for  $\psi(2S) \rightarrow \gamma\chi_{cJ} \rightarrow \gamma\gamma J/\psi \rightarrow \gamma\gamma\ell^+\ell^-$  [5] at the  $\psi(2S)$  peak, and a phase-space factor,  $F_X(s')$ , rescaling the latter to the actually produced mass of  $\psi(2S)$  at its resonance tail. Here,  $s$  is the center-of-mass energy (3773 MeV) squared,  $s'$  is the mass-squared with which the  $\psi(2S)$  resonance is produced, and  $x$  is the scaled radiated energy in  $e^+e^- \rightarrow \gamma\psi(2S)$ ,  $x = 1 - s'/s$ . Above, we have used the notation from Ref. [3], where the formula for  $W(s, x)$  is given and discussed in detail. Our selection cuts limit this radiated energy to less than 50 MeV ( $x < 0.027$ ), therefore, the  $\psi(2S)$  contribution is limited to its component which peaks near  $x \approx 0$ , where the energy resolution smears it to look like the  $\psi(3770)$  signal. The phase-space factor  $F_X(s')$  is equal to  $(E_\gamma(s')/E_\gamma^{\text{peak}})^3$  [6], where  $E_\gamma(s')$  and  $E_\gamma^{\text{peak}}$  are the energies of the photon in the  $\psi(2S) \rightarrow \gamma\chi_{cJ}$  transition at the  $\psi(2S)$  resonance tail ( $\sqrt{s'} \approx 3773$  MeV) and peak ( $\sqrt{s'} = M_R$ ), respectively. The  $\psi(2S)$  resonance mass ( $M_R$ ) and total width ( $\Gamma_R$ ) in the Breit-Wigner formula,  $BW(s') = 12\pi\Gamma_R\Gamma_{ee}/[(s' - M_R^2)^2 + M_R^2\Gamma_R^2]$ , are fixed to the world average values [7], while the  $\Gamma_{ee}$  is fixed to the value recently determined by CLEO [3]. Integrating the theoretical cross section in the  $x < 0.027$  range, and multiplying it by the event selection efficiencies given previously, we estimate that the  $\psi(2S)$  background contributes 12.2, 21.1 and 0.7 events to the  $\chi_{c2}$ ,  $\chi_{c1}$  and  $\chi_{c0}$  peaks, respectively. The systematic uncertainty in these estimates is 25%. We represent these background peaks in the fit to the energy spectrum by the same shapes as described previously for the signal contributions with the amplitudes fixed to the estimated number of background events.

The smooth background under the peaks is significantly higher in the  $\gamma\gamma e^+e^-$  sample than in the  $\gamma\gamma\mu^+\mu^-$  sample due to a high cross section for radiative Bhabha scattering. Therefore, instead of adding the photon energy distributions for these two samples, we fit them simultaneously, as illustrated in Fig. 3. The ratios of the peak amplitudes between the dimuon and dielectron samples are fixed to the ratios of the selection efficiencies. The signal shapes are constrained to be the same. The background-polynomial parameters are independent.

The fitted signal amplitudes (quoted for the sum of the dimuon and dielectron samples) are  $0.0_{-0.0}^{+2.9}$ ,  $53 \pm 10$  and  $22 \pm 9$  events for  $\chi_{c2}$ ,  $\chi_{c1}$  and  $\chi_{c0}$ , respectively. To estimate a probability that the data contain no signal contribution, we also perform fits with the signal

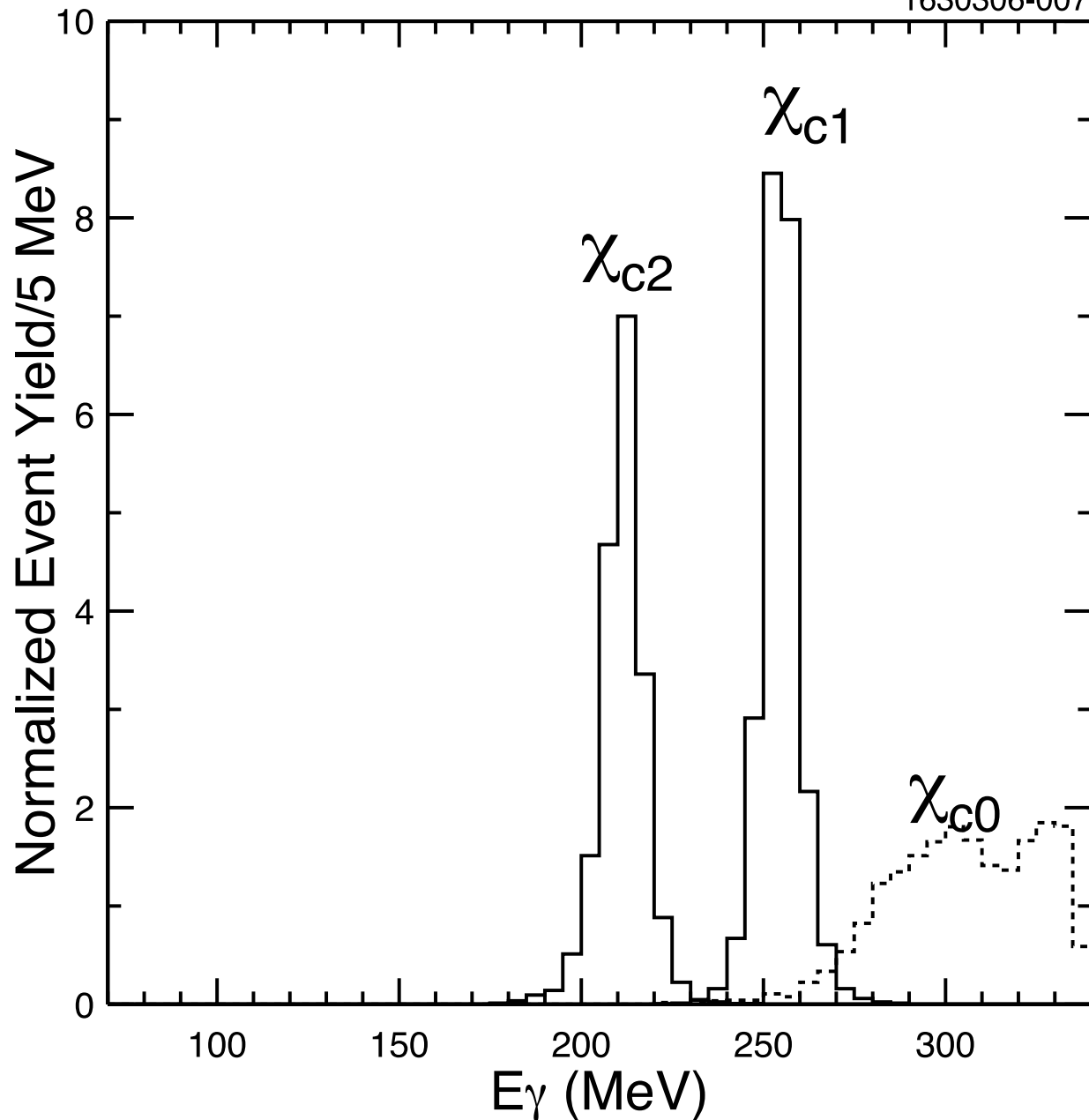


FIG. 2: Energy of the lower energy photon for the simulated  $\psi(3770) \rightarrow \gamma\chi_{cJ} \rightarrow \gamma\gamma J/\psi$ ,  $J/\psi \rightarrow \ell^+\ell^-$  events, for  $J = 2, 1$  (solid-line histograms) and 0 (dashed-line histogram). The vertical axis gives the number of detected Monte Carlo events per bin divided by the total number of generated events and then multiplied by a hundred. Thus, the area under each peak gives the detection efficiency in percent. The upper range of the horizontal axis reaches the kinematic limit.

amplitude fixed at zero. The ratio of the fit likelihoods is transformed into the number of standard deviations ( $\sigma$ ) at which the null hypothesis can be excluded, which, for our  $\psi(3770) \rightarrow \gamma\chi_{c1}$  signal, is  $6.6\sigma$ . The fitted peak energy,  $253.5 \pm 1.2$  MeV (statistical error only), is in excellent agreement with the 253.6 MeV value expected from the center-of-mass energy and the  $\chi_{c1}$  mass. The data in the  $\chi_{c1}$  signal region exhibit the expected peaking

TABLE I: Various quantities for  $\psi(3770) \rightarrow \gamma\chi_{cJ}$  transitions. Efficiencies given here are averaged over the  $\gamma\gamma\mu^+\mu^-$  and  $\gamma\gamma e^+e^-$  channels. The upper limits are at 90% C.L.

	$J = 2$	$J = 1$	$J = 0$
signal events	$0.0^{+2.9}_{-0.0}$	$53 \pm 10$	$22 \pm 9$
efficiency (%)	18	23	20
$\sigma(e^+e^- \rightarrow \psi(3770))$			
$\times \mathcal{B}(\psi(3770) \rightarrow \gamma\chi_{cJ})$ (pb)	$< 5.7$	$18.0 \pm 3.3 \pm 2.5$	$< 282$
$\mathcal{B}(\psi(3770) \rightarrow \gamma\chi_{cJ})$ (%)	$< 0.09$	$0.28 \pm 0.05 \pm 0.04$	$< 4.4$
$\Gamma(\psi(3770) \rightarrow \gamma\chi_{cJ})$ (keV)	$< 21$	$67 \pm 12 \pm 12$	$< 1050$

of the dilepton mass and of the two-photon recoil mass at the nominal  $J/\psi$  mass as shown in Fig. 4. Since the statistical significances of the  $\chi_{c2}$  and  $\chi_{c0}$  contributions are 0.0 and 1.7 standard deviations, respectively, there is no evidence for photon transitions via these states and we set upper limits on their rates.

The integrated luminosity of the datasets was measured using  $e^+e^-$ ,  $\mu^+\mu^-$  and  $\gamma\gamma$  events [8]; event counts were normalized with a Monte Carlo simulation based on the Babayaga [9] event generator. The resulting systematic error in luminosity measurement is 1%. The systematic error in efficiency simulation is 4%. Variations in the fit range, order of the background polynomial, bin size and the signal width result in a variation of the  $\chi_{c1}$  signal yield by 6%, while the systematic uncertainty in the subtraction of the  $\psi(2S)$  background contributes 7%. An additional systematic uncertainty of 6% comes from the  $\chi_{c1} \rightarrow \gamma J/\psi$  and  $J/\psi \rightarrow \ell^+\ell^-$  branching ratios [5] used in unfolding the measured rate for the  $\psi(3770) \rightarrow \gamma\chi_{c1}$  component. The systematic errors on the  $\chi_{c2}$  and  $\chi_{c0}$  rates are obtained in a similar way. To obtain upper limits, we combine statistical and systematic errors in quadrature. The results for  $\sigma(e^+e^- \rightarrow \psi(3770)) \times \mathcal{B}(\psi(3770) \rightarrow \gamma\chi_{cJ})$  are  $(18.0 \pm 3.3 \pm 2.5)$  pb for  $\chi_{c1}$ ,  $< 5.7$  pb (at 90% C.L.) for  $\chi_{c2}$ , and  $< 282$  pb (at 90% C.L.) for  $\chi_{c0}$ .

Using  $\sigma(e^+e^- \rightarrow D\bar{D})$  [10] for  $\sigma(e^+e^- \rightarrow \psi(3770))$ , given that all measured non- $D\bar{D}$  decays of  $\psi(3770)$  [3, 11] have very small cross sections, we obtain the following branching ratio results:  $\mathcal{B}(\psi(3770) \rightarrow \gamma\chi_{c1}) = (2.8 \pm 0.5 \pm 0.4) \times 10^{-3}$ ,  $\mathcal{B}(\psi(3770) \rightarrow \gamma\chi_{c2}) < 0.9 \times 10^{-3}$  (90% C.L.) and  $\mathcal{B}(\psi(3770) \rightarrow \gamma\chi_{c0}) < 44 \times 10^{-3}$  (90% C.L.).

We turn the branching ratio results into transition widths using  $\Gamma_{\text{tot}}(\psi(3770)) = (23.6 \pm 2.7)$  MeV [7]. This leads to:  $\Gamma(\psi(3770) \rightarrow \gamma\chi_{cJ}) = (67 \pm 12 \pm 12)$  keV for  $\chi_{c1}$ ,  $< 21$  keV (90% C.L.) for  $\chi_{c2}$ , and  $< 1.0$  MeV (90% C.L.) for  $\chi_{c0}$  (see Table I for the summary). These results agree well with most of the theoretical predictions [12, 13, 14] as shown in Table II.

Combining this measurement with our determination of the  $\pi^+\pi^- J/\psi$  rate [3] we obtain  $\Gamma(\psi(3770) \rightarrow \gamma\chi_{c1})/\Gamma(\psi(3770) \rightarrow \pi^+\pi^- J/\psi) = 1.49 \pm 0.31 \pm 0.26$  ( $> 1.0$  at 90% C.L.). The transition widths measured for  $\psi(3770)$ , which is predominantly the  $1^3D_1$  state, are theoretically related to the expected widths for the  $1^3D_2$  state. The ratio above is expected to be a factor 2-3.5 larger for the  $1^3D_2$  state with a mass of 3872 MeV than for the  $\psi(3770)$  [13, 15, 16]. In view of the upper limit from Belle,  $\Gamma(X(3872) \rightarrow \gamma\chi_{c1})/\Gamma(X(3872) \rightarrow \pi^+\pi^- J/\psi) < 0.9$  (90% C.L.) [1], the  $1^3D_2$  interpretation of  $X(3872)$  is strongly disfavored, which is also supported by other recent Belle results [17].

We gratefully acknowledge the effort of the CESR staff in providing us with excellent luminosity and running conditions. This work was supported by the National Science Foun-

TABLE II: Our measurements of the photon transitions widths (statistical and systematic errors have been added in quadrature) compared to theoretical predictions.

	$\Gamma(\psi(3770) \rightarrow \gamma\chi_{cJ})$ (keV)		
	$J = 2$	$J = 1$	$J = 0$
CLEO data	$< 21$	$67 \pm 17$	$< 1050$
Rosner [12]	$24 \pm 4$	$73 \pm 9$	$523 \pm 12$
Eichten-Lane-Quigg [13]			
naive	3.2	183	254
with coupled-channels corrections	3.9	59	225
Barnes-Godfrey-Swanson [14]			
non-relativistic potential	4.9	125	403
relativistic potential	3.3	77	213

dation and the U.S. Department of Energy.

- 
- [1] Belle Collaboration, S. K. Choi *et al.*, Phys. Rev. Lett. **91**, 262001 (2003).
  - [2] CDF-II Collaboration, D. Acosta *et al.*, Phys. Rev. Lett. **93**, 072001 (2004); D0 Collaboration, V.M. Abazov *et al.*, Phys. Rev. Lett. **93**, 162002 (2004); BaBar Collaboration, B. Aubert *et al.*, Phys. Rev. D **71**, 071103 (2005).
  - [3] CLEO Collaboration, N.E. Adam *et al.*, Phys. Rev. Lett. **96**, 082004 (2006).
  - [4] CLEO Collaboration, Y. Kubota *et al.*, Nucl. Instrum. Methods Phys. Res., **A320**, 66 (1992); D. Peterson *et al.*, Nucl. Instrum. Methods Phys. Res., **A478**, 142 (2002); M. Artuso *et al.*, Nucl. Instrum. Methods Phys. Res., **A554**, 147 (2005).
  - [5] CLEO Collaboration, Z. Li *et al.*, Phys. Rev. D **71**, 111103(R) (2005); N.E. Adam *et al.*, Phys. Rev. Lett. **94**, 232002 (2005).
  - [6] See e.g. Eq. (4.118) in N. Brambilla *et al.*, arXiv:hep-ph/0412158 (unpublished).
  - [7] Particle Data Group, S. Eidelman *et al.*, Phys. Lett. B **592**, 1 (2004).
  - [8] CLEO Collaboration, G. Crawford *et al.*, Nucl. Instrum. Methods Phys. Res., **A345**, 429 (1992).
  - [9] C.M. Carloni Calame *et al.*, Nucl. Phys. Proc. Suppl. B **131**, 48 (2004).
  - [10] CLEO Collaboration, Q. He *et al.*, Phys. Rev. Lett. **95**, 121801 (2005).
  - [11] CLEO Collaboration, G.S. Adams *et al.*, Phys. Rev. D **73**, 012002 (2006).
  - [12] J. L. Rosner, Phys. Rev. D **64**, 094002 (2001); J. L. Rosner, arXiv:hep-ph/0411003, Annals Phys. **319**, 1 (2005).
  - [13] E. J. Eichten, K. Lane and C. Quigg, Phys. Rev. D **69**, 094019 (2004).
  - [14] T. Barnes, S. Godfrey and E. S. Swanson, Phys. Rev. D **72**, 054026 (2005).
  - [15] E. J. Eichten, K. Lane and C. Quigg, Phys. Rev. Lett. **89**, 162002 (2002).
  - [16] T. Barnes and S. Godfrey, Phys. Rev. D **69**, 054008 (2004).
  - [17] Belle Collaboration, K. Abe *et al.*, hep-ex/0505037 (2005); hep-ex/0505038 (2005).



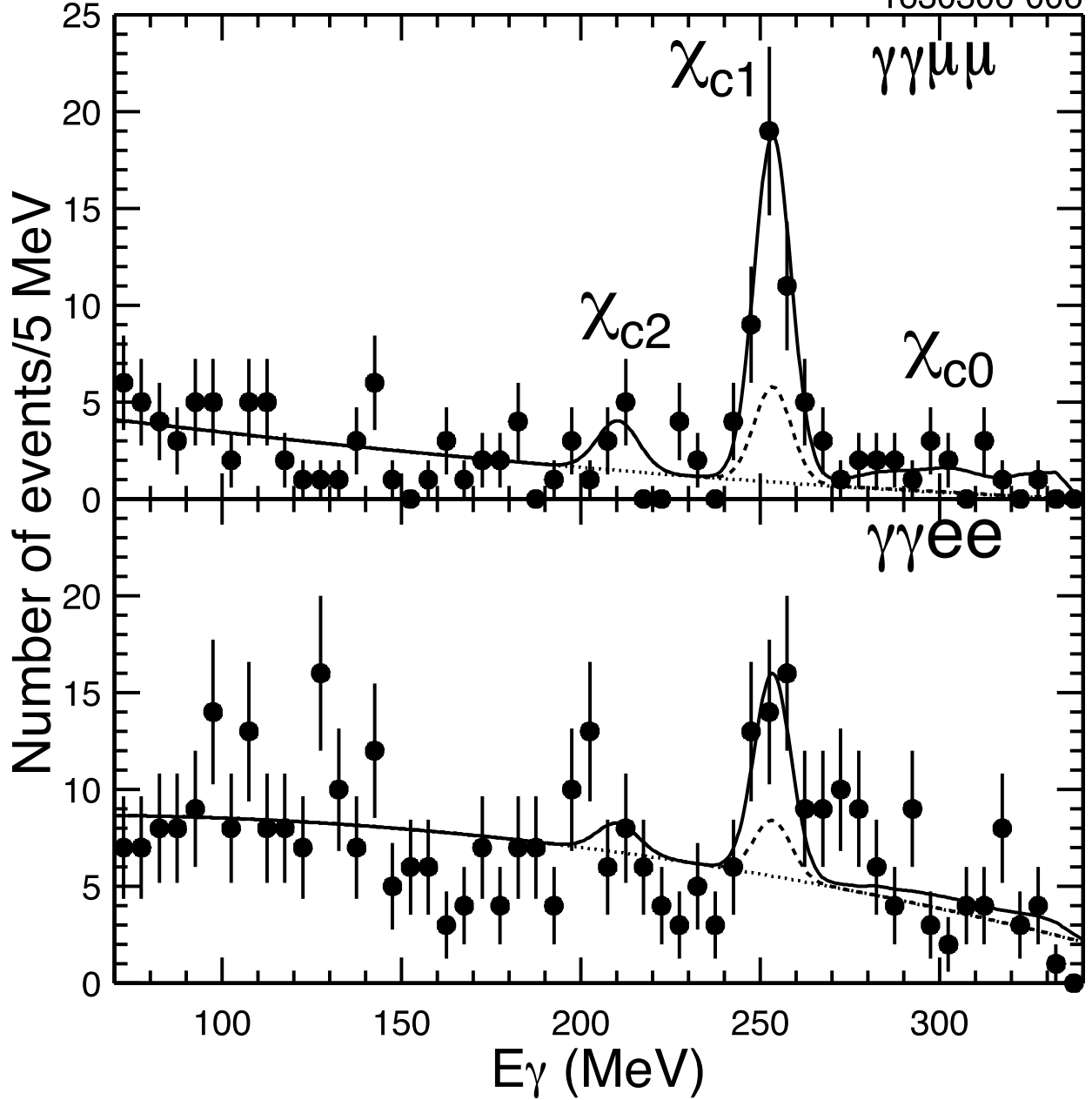


FIG. 3: Energy of the lower energy photon for the selected  $e^+e^- \rightarrow \gamma\gamma J/\psi$ ,  $J/\psi \rightarrow \mu^+\mu^-$  (top) and  $J/\psi \rightarrow e^+e^-$  (bottom) events at the  $\psi(3770)$  resonance. The solid line shows the fit. The dotted line shows the smooth background. The dashed line shows the total background including the expected background-peaks from radiatively produced tail of the  $\psi(2S)$  resonance (see text). The latter saturates the  $\chi_{c2}$  contribution. The excess in the  $\chi_{c1}$  peak above the  $2S$  contribution (dashed line) represents evidence for  $\psi(3770) \rightarrow \gamma\chi_{c1}$  transitions.

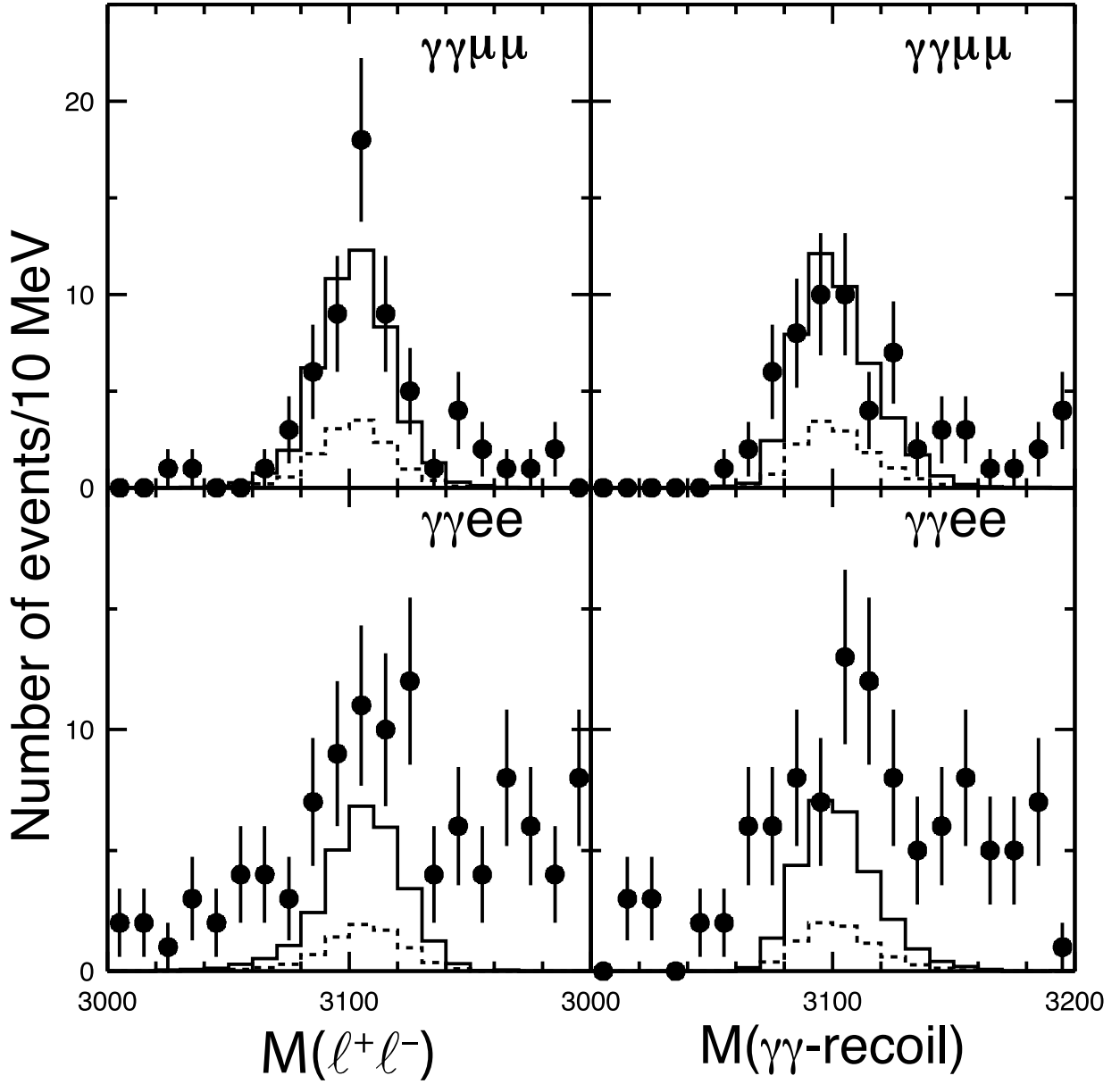


FIG. 4: Distributions of the  $J/\psi$  mass reconstructed either as dilepton mass (left plots) or diphoton recoil mass (right plots) for events with the lower photon energy within  $\pm 2\sigma$  of the  $\chi_{c1}$  peak. The cuts on both plotted quantities have been loosened to  $\pm 100$  MeV to avoid selection bias on the displayed distributions. The points with error bars represent the data. The dashed histograms represent the expected amount of  $\psi(2S) \rightarrow \gamma\chi_{c1}$  background. The solid histograms represent this background contribution plus the  $\psi(3770) \rightarrow \gamma\chi_{c1}$  signal contribution, as simulated with Monte Carlo, normalized to the number of signal events determined by the fit to the photon energy distribution. The  $\gamma\gamma e^+e^-$  data (bottom plots) have a higher level of other backgrounds and lower signal efficiency than the  $\gamma\gamma\mu^+\mu^-$  data (top plots).